Structural Eng./Earthquake Eng., JSCE, Vol. 17, No. 1, 21s−35s, 2000 April
(J. Struct. Mech. Earthquake Eng., JSCE, No. 647/I−51)

APPLIED ELEMENT METHOD FOR STRUCTURAL ANALYSIS: THEORY AND APPLICATION FOR LINEAR MATERIALS

Kimiro MEGURO[1] and Hatem TAGEL-DIN[2]

[1] Dr. of Eng., Associate Prof., International Center for Disaster-Mitigation Engineering (INCEDE), Institute of Industrial Science, The University of Tokyo
(4-6-1 Komaba, Meguro-ku, Tokyo 153-8505, Japan)
[2] Ph.D., Post-Doctorate Fellowship, Institute of Industrial Science, The University of Tokyo

A new method, Applied Element Method (AEM) for analysis of structures is introduced. The structure is modeled as an assembly of distinct elements made by dividing the structural elements virtually. These elements are connected by distributed springs in both normal and tangential directions. We introduce a new method by which the total behavior of structures can be accurately simulated with reasonable CPU time. This paper deals with the formulations used for linear elastic structures in small deformation range and for consideration of the effects of Poisson's ratio. Comparing with theoretical results, it is proved that the new method is an efficient tool to follow mechanical behavior of structures in elastic conditions.

Key Words: *Applied Element Method, AEM, confinement, Poisson's ratio, reinforced concrete, computer simulation*

1. INTRODUCTION

During earthquakes, buildings suffer from the different types of damage. Structure damage is classified into seven groups, as shown in **Table 1**, according to the AIJ[1]. In the first five groups, partial damage occurs to the structural and non-structural elements without collapse of the structure. Partial and complete collapse of structures is important topic under research because it causes extensive casualties inside and outside of the structures. In addition, collapse of a structure may lead to failure or collapse of near structures. Recent earthquakes, like Hyogo-Ken Nanbu Earthquake, show that structural failure was major cause of death toll[2]. Although this topic is very important for safety of people, current available methods for structural analysis can not deal with this problem accurately.

Numerical methods for structural analysis can be classified into two categories. In the first category, model is based on continuum material equations. The finite element method (FEM) is typical example of this category. Smeared Crack approach[3] can not be adopted in zones where separation occurs between adjacent structural elements. While, Discrete Crack Methods[3] assume that the location and direction of crack propagation are predefined before the analysis. With this group of the methods, analysis of structures, especially concrete structures, can be performed at most before collapse. The FEM can answer only the following question which is "Will the structure fail or not?" Unfortunately, it is very difficult to use the FEM for the second important question, which is "How does the structure collapse?" Although displacement of structural elements at failure may become tens of meters, analysis using the FEM could be performed till the start of failure, which means tens of centimeters at most.

The second group of methods uses the discrete element techniques, like the Rigid Body and Spring Model (RBSM)[4] and the Extended Distinct Element Method (EDEM[5, 6]). The main advantage of these methods is that they can simulate the cracking process with relatively simple technique compared to the FEM, while the main disadvantage is that crack propagation depends mainly on the element shape, size and arrangement[7, 8]. Analysis using the RBSM could not be performed up to complete collapse of the structure. On the other hand, the EDEM can follow the structural behavior from zero loading and up to complete collapse of the structure. However, the accuracy of EDEM in small deformation range is less than that of the FEM.

Table 1 Damage level of structures as defined by the AIJ[1)]

Damage level	*Damage of members*
1- No damage	No damage is found.
2- Slight damage	Columns, shear walls or non-structural walls are slightly damaged.
3- Light damage	Columns or shear walls are slightly damaged. Some shear cracks in non-structural walls are found.
4-Moderate damage	Typical shear and flexural cracks in columns, shear cracks in shear walls, or severe damage in non-structural walls are found.
5- Heavy damage	Spalling of concrete, buckling of reinforcement, and crushing or shear failure in columns are found. Lateral resistance of shear walls is reduced due to heavy shear cracks.
6- Partial collapse	The building is partially collapsed due to severely damaged columns and/or shear walls.
7- Total collapse	The building is totally collapsed due to severely damaged columns and/or shear walls.

Table 2 Organization of research results

		Static		Dynamic	
Geometry	*Material*	*Monotonic*	*Cyclic*	*Monotonic*	*Cyclic*
Small deformation (linear)	*Elastic*	I(This paper)	III[12)]	V[13)]	VI[14)]
	Nonlinear	II[10)]			
Large deformation (nonlinear)	*Elastic*	IV[11)]			
	Nonlinear	Covered in dynamics			
Collapse process		No meaning			

Hence, the failure behavior obtained by repeated many calculations is affected due to cumulative errors and can not be predicted accurately using the EDEM. This means that the EDEM can answer only the second question, "How does the structure collapse?"

From the fact discussed above, we can say that there is no proper method among current available techniques by which total behavior of structures from zero loading to collapse can be followed with reliable accuracy and reasonable CPU time.

The major advantages of the proposed method are simple modeling and programming, and high accuracy of the results with relatively short CPU time. Using the method, highly nonlinear behavior, i.e. crack initiation, crack propagation, separation of structural elements, rigid body motion of failed elements and totally collapse process of the structure can be followed with high accuracy[9)].

To cover a wide range of applications, analyses should be performed for different fields of application. The main factors affecting structural analysis can be categorized as:

1. Effects of inertia forces: The loading types are divided into two categories, static and dynamic loading conditions. In dynamic loading case, the inertia and damping forces should be taken into account and hence, loading is a function of time.
2. Effects of the direction of loading: The analyses are divided into two categories, monotonic and cyclic loading conditions. In monotonic loading condition, the load direction is constant while its value increases, and in case of cyclic loading, the load direction and values are changing.
3. Effects of geometrical changes: In some analyses, the deformations are considered small with respect to the structural dimensions. It can be assumed that the structure geometry is constant and effects of geometrical changes on the stiffness matrix or internal forces are neglected. In other cases, like buckling cases, deformations are large and geometrical nonlinear behavior should be discussed.
4. Effects of material properties: The material behavior can be assumed as linear or nonlinear behavior. In linear behavior, all stress-strain relations are constant. In nonlinear case, cracking, yield of the material and nonlinear stress-strain relations should be considered.

The organization of the research is shown in **Table 2**. This table shows all meaningful application ranges which could be covered by the proposed numerical model together with the corresponding reference. The dark area indicates that there is no meaning to perform simulation, like simulation of collision effects in static loading condition. In the lightly hatched area, application in static loading conditions is not reasonable because in case of nonlinear material, structural elements, like concrete elements in large deformation range, tend to separate. This indicates that the effects of inertia forces and rigid body motions become dominant. Therefore, this range is covered in dynamics.

Main purposes of the paper are a) introduction of background and outline of newly proposed model, AEM, and b) formulation of fundamental parts of the AEM. This is the first paper in a series of papers

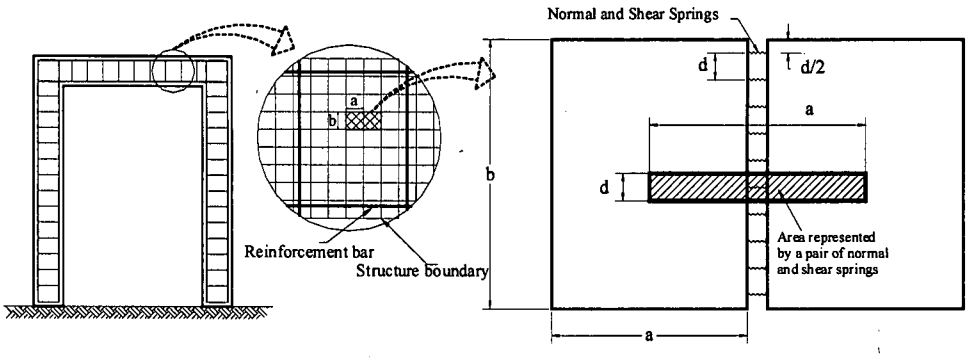

(a) Element generation for AEM

(b) Spring distribution and area of influence of each pair of springs

Fig. 1 Modelling of structure to AEM

that cover all the application ranges shown in **Table 2**. Because of the limitation of the number of pages, authors will publish whole research work through several journal papers. In this paper, formulations and verifications of the numerical technique in case of elastic-static loading condition is introduced. In additions, the effects of element size and number of connecting springs is discussed. Moreover, the numerical procedures to consider Poisson's ratio effects are introduced.

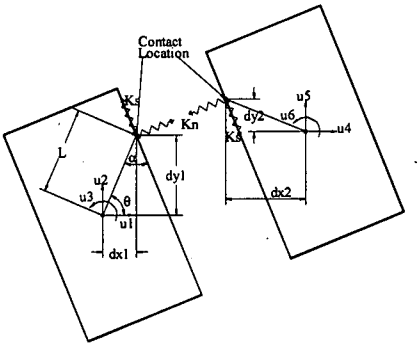

Fig. 2 Element shape, contact location and degrees of freedom

2. ELEMENT FORMULATION

With the AEM, structure is modelled as an assembly of small elements which are made by dividing of the structure virtually, as shown in **Fig. 1 (a)**. The two elements shown in **Fig. 1** are assumed to be connected by pairs of normal and shear springs located at contact locations which are distributed around the element edges. Each pair of springs totally represent stresses and deformations of a certain area (hatched area in **Fig. 1 (b)**) of the studied elements. The spring stiffness is determined as shown in Eq. (1):

$$K_n = \frac{E \times d \times T}{a} \text{ and } K_s = \frac{G \times d \times T}{a} \qquad (1)$$

where, d is the distance between springs, T is the thickness of the element and "a" is the length of the representative area, E and G are the Young's and shear modulus of the material, respectively. The above equation indicates that each spring represents the stiffness of an area (d x T) with length "a" of the studied material. In case of reinforcement, this area is replaced by that of the reinforcement bar. The above equation indicates that the spring stiffness is calculated as if the spring connects the element centerlines.

Three degrees of freedom are assumed for each element. These degrees of freedom represent the rigid body motion of the element. Although the element motion is a rigid body motion, its internal stress and deformations can be calculated by the spring deformation around each element. This means that although the element shape doesn't change during analysis, the behavior of assembly of elements is deformable. The Poisson's ratio effect, which is not considered in this formulation, is illustrated in details in Section (6).

The two elements shown in **Fig. 2** are assumed to be connected by only one pair of normal (stiffness: Kn) and shear (stiffness: Ks) springs. The values of (dx and dy) correspond to the relative coordinate of the contact point with respect to the centroid. To have a general stiffness matrix, the location of element and contact springs are assumed in a general position. The stiffness matrix components corresponding to each degree of freedom are determined by assuming a unit displacement in the studied direction and by determining forces at the centroid of each element. The element stiffness matrix size is only (6 x 6). Equation (2) shows the components of the upper left quarter of the stiffness matrix. All used notations in this equation are

shown in **Fig. 2**. It is clear that the stiffness matrix depends on the contact spring stiffness and the spring location.

$$\begin{bmatrix} \begin{matrix}\sin^2(\theta+\alpha)K_n \\ +\cos^2(\theta+\alpha)K_s\end{matrix} & \begin{matrix}-K_n\sin(\theta+\alpha)\cos(\theta+\alpha) \\ +K_s\sin(\theta+\alpha)\cos(\theta+\alpha)\end{matrix} & \begin{matrix}\cos(\theta+\alpha)K_sL\sin(\alpha) \\ -\sin(\theta+\alpha)K_nL\cos(\alpha)\end{matrix} \\ \begin{matrix}-K_n\sin(\theta+\alpha)\cos(\theta+\alpha) \\ +K_s\sin(\theta+\alpha)\cos(\theta+\alpha)\end{matrix} & \begin{matrix}\sin^2(\theta+\alpha)K_s \\ +\cos^2(\theta+\alpha)K_n\end{matrix} & \begin{matrix}\cos(\theta+\alpha)K_nL\cos(\alpha) \\ +\sin(\theta+\alpha)K_sL\sin(\alpha)\end{matrix} \\ \begin{matrix}\cos(\theta+\alpha)K_sL\sin(\alpha) \\ -\sin(\theta+\alpha)K_nL\cos(\alpha)\end{matrix} & \begin{matrix}\cos(\theta+\alpha)K_nL\cos(\alpha) \\ +\sin(\theta+\alpha)K_sL\sin(\alpha)\end{matrix} & \begin{matrix}L^2\cos^2(\alpha)K_n \\ +L^2\sin^2(\alpha)K_s\end{matrix} \end{bmatrix} \quad (2)$$

The stiffness matrix in Eq. (2) is for only one pair of contact springs. However, the global stiffness matrix is determined by summing up the stiffness matrices of individual pair of springs around each element. Consequently, the developed stiffness matrix is an average stiffness matrix for the element according to the stress situation around the element. This technique can be used both in load and displacement control cases. The governing equation is

$$[K_G][\Delta] = [F] \quad (3)$$

where, $[K_G]$ is the global stiffness matrix; $[\Delta]$ the displacement vector and $[F]$ the applied load vector. In load control case, the vector, $[F]$, is known before the analysis. In displacement control case, the load is applied by unit virtual displacement for one or more degrees of freedom.

3. PROGRAM COMPOSITION

The flow chart of the method in elastic loading condition is shown in **Fig. 3**. As the numbers of elements and connecting springs are large, in the program, the element location and spring data are automatically generated based on the reinforcement details of the structure before the analysis. In case of reinforced concrete (RC) structures, the coordinates of the springs representing the reinforcement bars are defined by the nearest spring. For horizontal reinforcement, "Y" coordinate is defined while for vertical reinforcement, "X" coordinate is set. At the location of reinforcement bar, two springs are set. The first one is for steel bar while the other is for concrete. It is assumed that both springs have the same strain at each loading stage.

The idea of this technique is based on transforming the global stiffness matrix, whose size is (N x N), to another vector whose elements are the non-zero elements of half of the original matrix, as it is symmetrical. The solution of equations is applied to the new vector. This technique has the advantages that the memory capacity required for storing the stiffness matrix data can be reduced and that CPU time required for solving the equations is drastically reduced because the calculations are performed only to the non-zero elements. This

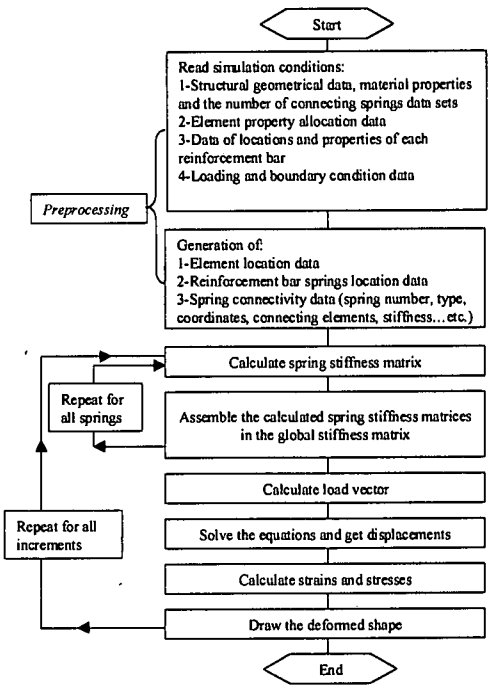

Fig. 3 Flow chart of the program

advantage is very important in nonlinear analysis as the stiffness matrix is reconstructed and solved during each increment.

4. EFFECT OF NUMBER OF CONNECTING SPRINGS BETWEEN ELEMENTS

The number of connecting springs between elements is one of the key factors that should be taken into account. Obviously, in nonlinear analysis, increasing the number of connecting springs between elements leads to better results of crack propagation. This section shows that the number of connecting springs should be determined carefully even in elastic analysis. Referring to **Fig. 4**, it is assumed that "2n" springs are connecting two elements together. Each spring represents the stiffness of a distance of (b/2n). In translational degrees of freedom case, the number of connecting springs has no effect on the element stiffness as decreasing the number of connecting springs leads to increasing of area represented by each spring. Finally, the total area becomes as the same as that represented by one whole element. It means that one spring can represent totally translational degrees of freedom of an element but cannot do rotational degree of freedom. Rotation of an element has effect due to the number of springs and it is mainly resisted by shear springs together with normal

springs. Theoretical rotational stiffness, K_r, calculated from normal springs is:

$$K_r = \int_{y=-b/2}^{y=b/2} \frac{ET}{b} \times z \times z \times dz = \frac{ETb^2}{12} \quad (4)$$

where T is the element thickness and E is the Young's modulus. The element rotational stiffness is obtained by summing up all the rotational stiffness calculated for each spring separately. It can be proved easily that the total rotational stiffness is:

$$K_r = \frac{ETb^2}{4n^3} \sum_{i=1}^{n} (i - 0.5)^2 \quad (5)$$

where "i" is the spring number. Referring to the Eq. (5), the calculated rotational stiffness is a function of the number of connecting springs. **Table 3** shows the relation between the number of connecting springs and the percentage of error between the theoretical and calculated results. From **Table 3**, in case of two connecting springs, the numerically obtained rotational stiffness is smaller than the theoretical value by 25% which is quite large. However, this error reduces to less than 1% if the number of connecting springs is 10 or more. This effect is dominant if the element size is relatively large compared to the structure size. The error vanishes when the element size is small because the relative rotation between adjacent elements becomes small.

5. EFFECT OF ELEMENT SIZE

Adjustment of element size in the analysis is very important. Simulation of structures using elements of large size leads to increasing the structure stiffness and failure load of structure. This means that the calculated displacements become smaller and the failure load gets to be larger than the actual one. To make this effect clear, we carried out a series of simulations using the laterally loaded cantilever models as shown in **Fig. 5**. The dimensions of the models are also shown in the figure. The Young's modulus is assumed as 2.1×10^8 kN/m^2 and elastic analysis was performed using the proposed method. The lateral load value is taken as 10kN and column thickness is 0.25m. The results were compared with the theoretical results of elastic structure. The percentage of error in maximum displacement and the CPU time (CPU: DEC ALPHA 300 MHz) are shown in **Fig. 6**.

To discuss the effect of the number of connecting springs, the analyses were performed using two models with 20 and 10 springs connecting each pair

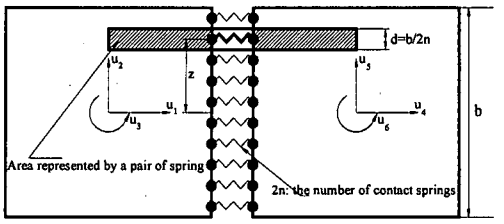

Fig. 4 Effect of the number of connecting springs on rotational stiffness

Table 3 Relation between the number of connecting springs and the calculated error in rotational stiffness

(2n)	2	4	6	8	10	20
Error ratio (%) $[((K_r^n/K_r^t)-1)*100]$	25	6.3	2.8	1.6	1.0	0.3

of adjacent element faces for each case of different element size. From the figure, it is evident that increasing the number of base elements leads to decreasing the error but increasing the CPU time. Use of only one element at the base leads to about 30% error of theoretically calculated displacement. This error reduces to less than 1% when the number of elements at the base increases to 5 or more. However, the CPU time increases rapidly. When we compare the results using 20 and 10 springs, although the CPU time in case of 10 springs is almost half of that in case of 20 springs, the accuracy of the results of 10 springs model is same as that in case of 20 springs. From this figure, it can be concluded that usage of large number of elements together with relatively few number of connecting springs leads to high accuracy in reasonable CPU time. To improve the accuracy in case of elastic analysis, it is advisable to increase the number of elements rather than increasing the number of connecting springs.

Figures 7 and **8** show the normal and shear stresses distribution at the base of the studied columns for different number of base elements. From these figures, the followings should be noticed:

- Calculated normal stresses are very close to the theoretical values even in case of the smaller number of elements at the base.
- Shear stress values are constant for the same element.
- Shear stress values are far from the theoretical values in case of the smaller number of elements at the base and become close to the theoretical results as the number of elements increases.

This means that behavior in which the effect of shear stresses is minor, like the case of slender frames, can be simulated by elements of relatively large size. To improve the accuracy of analysis

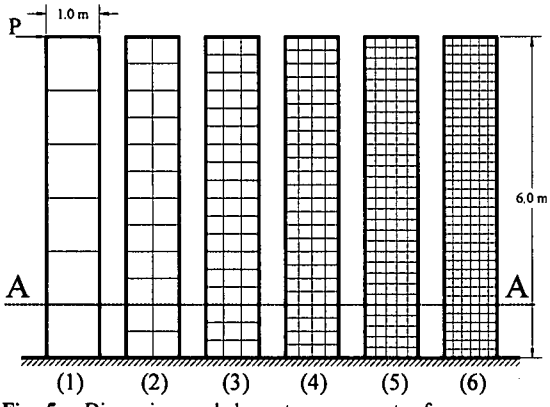

Fig. 5 Dimensions and element arrangements of laterally loaded cantilever models

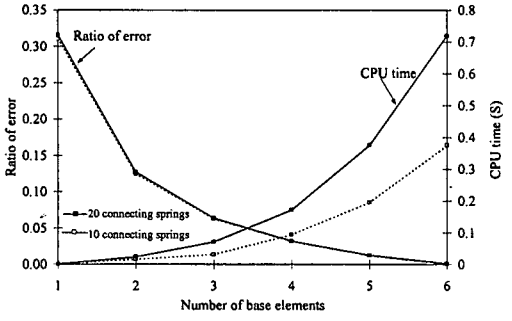

Fig. 6 Relations between the number of base elements, ratio of error and CPU time

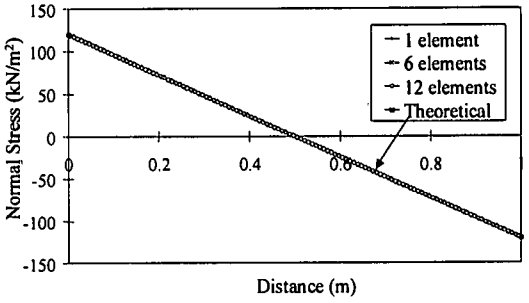

Fig. 7 Normal stress distribution at section A-A

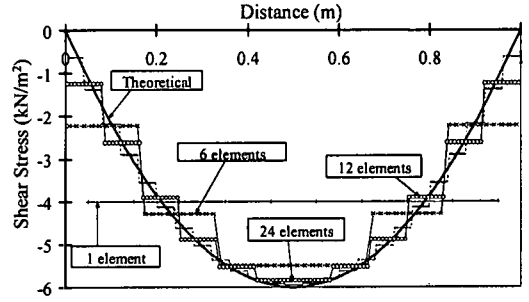

Fig. 8 Shear stress distribution at section A-A

using elements of large size, attention should be paid for the unsupported length, which is total length without the length of elements at the base. On the other hand, in case of walls and deep beams, elements of small size should be used to follow the fracture behavior in the shear dominant zones.

6. POISSON'S RATIO EFFECT

(1) Introduction

Although there are many phenomena in which the effects of Poisson's ratio are minor, in some cases, Poisson's ratio plays an essential role governing the phenomena. For example, the effect of lateral confinement for columns subjected to axial forces is a typical case. This effect can be taken into account using FEM, however, failure behavior can not be properly followed using the FEM after separation of structural members. Recently, many other methods were developed to deal with fracture behavior problems, like the RBSM[4), 7), 8)] and the EDEM[5), 6)]. However, the effects from Poisson's ratio were not taken into account in these methods. This section introduces a new technique to deal with the effects due to Poisson's ratio.

Referring to **Fig. 1(b)**, vertical deformations obtained on vertical edges do not affect the horizontal deformations. This indicates that elements are rigid and no lateral deformations are transformed through element edges. This is equivalent to having zero Poisson's ratio value. The main objective of this section is to introduce how to transform element behavior from rigid body state to a flexible state. To consider the effects due to Poisson's ratio, two main approaches can be adopted. The first approach is by adding two degrees of freedom to the elements in 2-D as shown in **Fig. 9**. The total number of degrees of freedom increases from 3 to 5 for each element. Three degrees of freedom (u, v and r) are for rigid body motion of the element and additional two components (uu and vv) are the relative deformations between the vertical and horizontal edges. The uu and vv correlate the deformations of element edges based on Poisson's ratio. Adding these effects to the stiffness matrix proposed in Eq. (2), the effects of Poisson's ratio can be considered. Although this approach is applicable, it has two main disadvantages:

- A coupling effect occurs among the degrees of freedom representing the rigid motion of elements and those representing the relative

deformations between element edges. This effect makes the calculation of strains and stresses very difficult in comparison with the case where the Poisson's ratio effect is not considered.

- The number of degrees of freedom increases from 3 to 5. This means that the time for assembling the stiffness matrix and for solving the equations gets to be longer than double [$\approx(5/3)^2$]. Moreover, the computer memory capacity required also drastically increases.

The second approach, which is adopted here, is simple and does not have the disadvantages of the first approach. By the second approach, the Poisson's ratio effect can be taken into account even when three degrees of freedom are used. Although the element moves as a rigid body, assembly of elements is deformable. The idea is simply adopted by correlating the stiffness matrix of each element by those of adjacent elements. The idea is illustrated in the next sections.

(2) Geometrical definitions

Assume the elements arrangement shown in **Fig. 10 (a)**. As a general case, the element (0) is surrounded by eight elements. Each element has three degrees of freedom and four edges numbered from 1 to 4, refer to **Fig. 10 (b)**. The factors "f" shown in **Fig. 10 (a)** and Eq. (6) represent the element continuity which will be illustrated in the following sections:

$$fijk=fij \times fik \qquad (6)$$

where, "i" is the element number, j and k represent edge numbers. The factor "fij" is equal to one if connecting springs of element "i" at the edge "j" exist, like "f52" and "f53". If there is no element connected with the element "i", at the edge "j" or the springs are failed because of cracks, "fij" is set to zero, like "f51" and "f54". This means that "fijk" is equal to one when the connection of the element "i" at the edges "j" and "k" is valid, like "f523". Otherwise, "fijk" is equal to zero, like "f512", "f534" and "f541". These factors are used to develop the stiffness matrix which enables us to take into account the effects of Poisson's ratio in general for any element configuration.

(3) Numerical analysis procedure

The original stiffness matrix, which does not take into account the effects of Poisson's ratio, is developed by summing the stiffness matrices of springs around each element. Additional terms are adopted to consider the Poisson's ratio. For each degree of freedom, the additional stiffness matrix terms are developed by assuming a corresponding

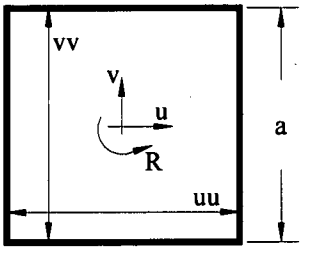

Fig. 9 Suggested degrees of freedom to consider Poisson's ratio effect

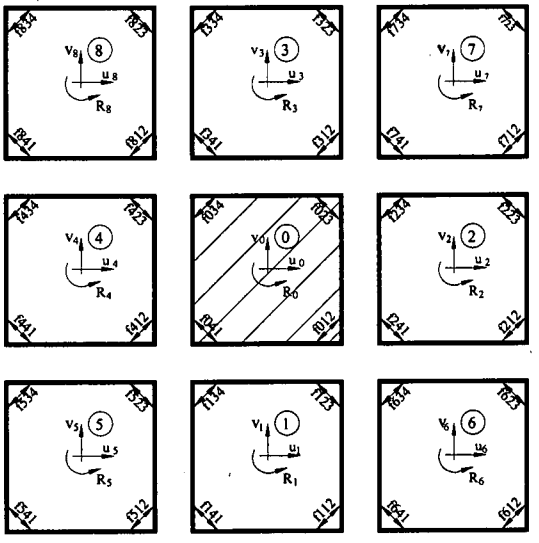

(a) Element configuartion

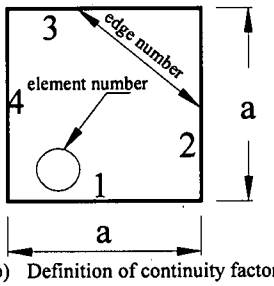

(b) Definition of continuity factor

Fig. 10 Element configuration and the definition of continuity factors

displacement in the direction of the studied degree of freedom and calculating the reactions at the centroid of each surrounding element. **Figure 11** shows the additional terms corresponding to horizontal displacement of element (0). While, **Fig. 12** deals with vertical displacement. **Figures 13 (a)** and **13 (b)** deal with rotational degree of freedom. These terms are added directly to the global stiffness matrix.

Referring to **Fig. 11**, horizontal displacement is applied to the element (0). All other degrees of freedom are restrained. Springs between the

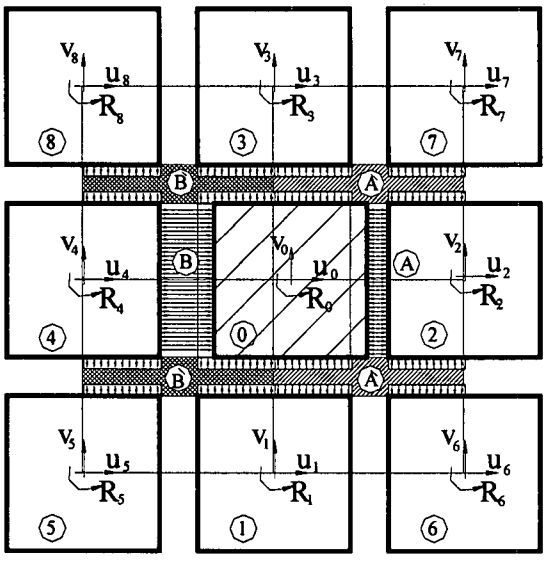

Fig. 11 Secondary stresses due to horizontal displacement of the element (0)

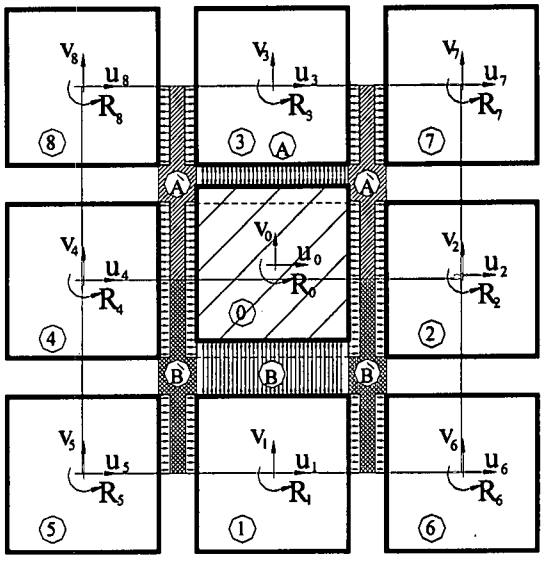

Fig. 12 Secondary stresses due to vertical displacement of the element (0)

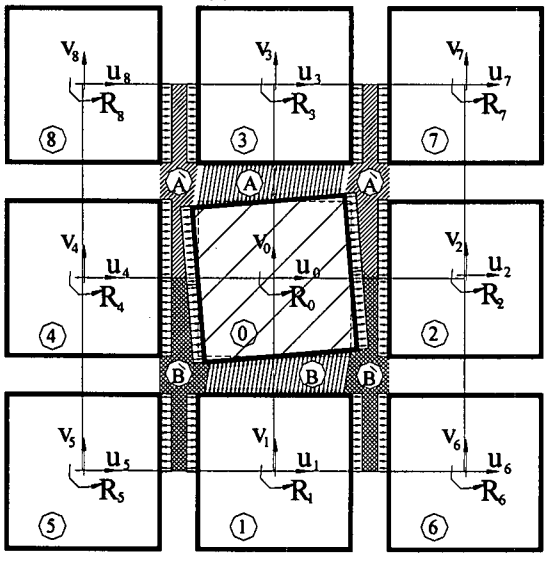

(a) Effect of rotation of horizontal edges on stresses of vertical edges

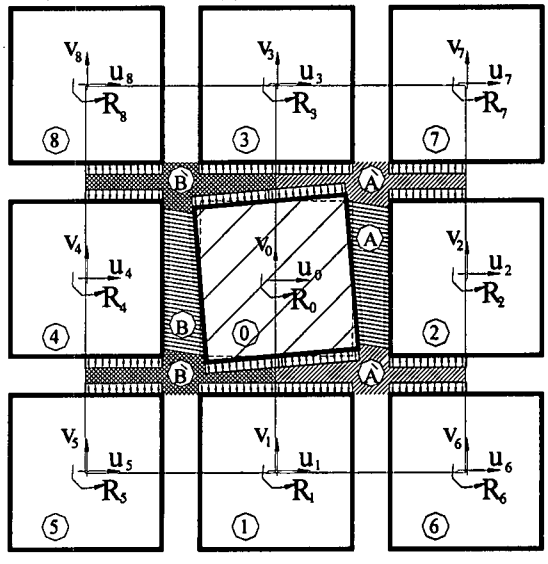

(b) Effect of rotation of vertical edges on stresses of vertical edges

Fig. 13 Secondary stresses due to rotational displacement of the element (0)

elements (0 and 2) are subjected to compression. The area represented by the compressed springs, group "A", is the right half of the element (0) and the left half of the element (2). Compression forces (horizontal) between the elements (0 and 2) leads to lateral (vertical) displacement for the area represented, group "A\".

This lateral displacement is a function of Poisson's ratio. As this lateral displacement is prevented, because all degrees of freedom of other elements are assumed to be restrained, additional stresses are produced in zone "A\". These additional stresses are assumed to be uniform over the element edges. The additional stresses are transformed to the center of elements as force and moment, and added to the global stiffness matrix. When one of surrounding elements does not exist, the calculated secondary stresses change. For example, stress components between the elements (2 and 6) exist if the connection between the elements (0 and 2) and (2 and 6) are valid. This means that elements exist and springs are not cracked. For instance, if the element (6) does not exist, no additional stress component on the element (2) is used. This means that "f21" (edge 1 of the element 2) is equal to zero. The stiffness matrix components corresponding to

Table 4 Added stiffness matrix values due to unit displacement of each degree of freedom of element (0)

(0)			(1)			(2)		
u0	**v0**	**R0**	**u1**	**v1**	**R1**	**u2**	**v2**	**R2**
0	p0 x (-f012+f023 -f034+f041)	m0 x (-f012+f023 +f034-f041)	0	p0 x (+f012-f041)	m0 x (+f012+f041)	0	p2 x (-f241+f234)	m2 x (+f241-f234)
p0 x (-f012+f023 -f034+f041)	0	m0 x (-f012-f023 +f034+f041)	p1 x (-f123+f134)	0	m1 x (+f123-f134)	p0 x (+f012-f023)	0	m0 x (+f012+f023)
m0 x (-f012+f023 +f034-f041)	m0 x (-f012-f023 +f034+f041)	-2 x m0 x a/4 (f012+f023 +f034+f041)	m1 x (-f123-f134)	m0 x (+f012-f041)	a/4 x (+m0 x f012 +m0 x f041 +m1 x f123 +m1 x f134)	m0 x (f012-f023)	m2 x (-f241-f234)	a/4 x (+m2 x f241 +m2 x f234 +m0 x f012 +m0 x f023)

(3)			(4)			(5)		
u3	**v3**	**R3**	**u4**	**v4**	**R4**	**u5**	**v5**	**R5**
0	p0 x (-f023+f034)	m0 x (-f023-f034)	0	p4 x (+f412-f423)	m4 x (+f412-f423)	0	-p4 x f412	-m4 x f412
p3 x (+f312-f341)	0	m3 x (+f312-f341)	p0 x (-f041+f034)	0	m0 x (-f041-f034)	-p1 x f134	0	m1 x f134
m3 x (+f312+f341)	m0 x (+f023-f034)	a/4 x (+m0 x f023 +m0 x f034 +m3 x f312 +m3 x f341)	m0 x (+f041-f034)	m4 x (+f412+f423)	a/4 x (+m4 x f412 +m4 x f423 +m0 x f041 +m0 x f034)	m1 x f134	m4 x -f412	a/4 x (-m4 x f412 -m1 x f134)

(6)			(7)			(8)		
u6	**v6**	**R6**	**u7**	**v7**	**R7**	**u8**	**v8**	**R8**
0	+p2 x f241	-m2 x f241	0	-p2 x f234	+m2 x f234	0	+p4 x f423	+m4 x f423
+p1 x f123	0	-m1 x f123	-p3f312	0	-m3 x f312	+p3f341	0	+m3 x f341
+m1 x f123	+m2 x f241	a/4 x (-m2 x f241 -m1 x f123)	-m3 x f312	+m2 x f234	a/4 x (-m2 x f234 -m3 x f312)	-m3 x f341	-m4 x f423	a/4 x (-m4 x f423 -m3 x f341)

the applied unit displacements are determined by transmitting the calculated secondary stresses to the centroids of the corresponding elements.

In case that springs between the elements (0 and 4) are subjected to tension, group "B", the area represented by the springs subjected to tension is the left half of the element (0) and the right half of the element (4). Tension forces (horizontal) between the elements (0 and 4) leads to lateral (vertical) displacement for the area represented, group "B'". Additional stresses exist in zone "B'".

The calculated additional stresses are based only on assumption that the element (0) is surrounded by elements from all directions. For example, if the element (8) does not exist, no stress component exists between the elements (4 and 8). This means that lateral displacement is permitted in the upper edge of the element (4). To make the technique general, the calculated reaction component is multiplied by a continuity factor representing the continuity condition of each element edge.

Referring to **Fig. 12**, the same technique can be applied to the vertical displacement component of the element (0). **Figure 13 (a)** shows the effect of rotation of horizontal edges of the element (0) while **Fig. 13 (b)** shows the effect of rotation of vertical edges. In all the cases, secondary stresses, calculated in case of element rotation, are assumed to be uniformly distributed over the element edges as only one degree of freedom is assumed for each direction in an element.

Global stiffness matrix should be modified to add the consideration of the effects of the Poisson's ratio as shown in **Table 4**. The effects of Poisson's ratio due to unit displacement of each degree of freedom of the element (0) on the other surrounding elements are shown in the table. The transmitted force and moments "pi" and "mi" are defined as:

$$pi = \frac{\nu \times E_i \times t_i}{4(1-\nu^2)} \quad \text{and} \quad mi = \frac{\nu \times E_i \times t_i}{4(1-\nu^2)} \times \frac{a}{4} \qquad (7)$$

where, "ν" is Poisson's ratio; "E" the Young's modulus; "t" the element thickness; "a" the element size. The subscript "i" is the element number.

It can be noticed from **Table 4** that the stiffness matrix is general for any element configuration due to the use of element continuity factors. If one of neighboring elements does not exist, its effect on the stiffness matrix is automatically removed.

Calculation algorithm of stresses is different from that in case of perfectly rigid elements. In case of perfectly rigid elements, stresses are proportional to the relative displacement between the two ends of

each spring. When the effects of Poisson's ratio are considered, the following technique is adopted after assembling the global stiffness matrix and solution of equations:

1. For each spring, calculate the strain from the displacements of spring ends, ε_x and ε_y by:

$$\varepsilon_x = \frac{d_x}{a} \text{ and } \varepsilon_y = \frac{d_y}{a} \quad (8)$$

where d_x and d_y are relative displacements of spring ends in x and y directions, respectively. For each spring, either ε_x or ε_y can be calculated. The same formula is used for calculation of strain in case of perfectly rigid elements.

2. Calculate the average strains (ε_{xa} or ε_{ya}) for each element in x and y directions, and
3. Calculate the concrete stresses for each spring in x and y directions, ε_x and ε_y, from Eq.(9), where E_c is Young's Modulus for concrete.

$$\sigma_x = E_c \times \left(\varepsilon_x + \upsilon\varepsilon_{ya}\right)/\left(1-\upsilon^2\right)$$
$$\sigma_y = E_c \times \left(\varepsilon_y + \upsilon\varepsilon_{xa}\right)/\left(1-\upsilon^2\right) \quad (9)$$

4. Calculate the reinforcement stresses for each spring in x and y directions from Eq.(10), where E_s is Young's Modulus for steel.

$$\sigma_x = E_s \times \varepsilon_x \text{ and } \sigma_y = Es \times \varepsilon_y \quad (10)$$

It should be mentioned that if Poisson's ratio is set equal to zero, the stress-strain relation becomes simpler and no coupling between stresses in both direction occurs.

(4) Verification of the proposed technique

The numerical technique proposed is verified by analyzing elastic prism specimen subjected to uniform compression. Simulations are carried out using two models with and without friction between loading plates and specimen. The size of the specimens is (20x36) cm with unit thickness. The loading plate thickness is assumed 2.0 cm and its stiffness is much higher than that of the prism so that effects of deformations of these plates compared with that of the specimens are neglected. Analysis is performed under assumption of plane stress condition for only one quarter of the model. The applied stresses in all cases are the same. The Poisson's ratio is varied from 0 to 0.5 with 0.1 increment. The friction between the loading plates and the specimens are assumed zero in the first cases, while in the second cases, shear springs with the stiffness of 40% of the normal springs are used in the interface between the loading plates and the prisms.

Figure 14 shows the deformed shape in cases where no friction exists between the loading plates and the specimen. Displacements are generally uniform in the specimen. Increasing the Poisson's ratio leads to increasing the horizontal displacements. Although the lateral displacement of the specimens increases with increasing the Poisson's ratio, the vertical displacements are the same. This agrees well with the theory, as there is no lateral stresses applied to the specimens. From the simulated vertical and horizontal displacements, Poisson's ratios are calculated and compared with the theoretical ones in **Fig. 15**. The results show good agreement with theoretical results and the maximum difference between the theoretical and calculated values is less than 1%. This gives evidence that the numerical technique proposed is accurate enough and can be applied to structural phenomena governed by the Poisson's ratio.

Figure 16 shows the deformed shapes in cases of the specimen having different Poisson's ratios where friction exists. In case when the Poisson's ratio, ν, equals to zero, no horizontal displacement exists. On the other hand, lateral displacement is maximum when ν is equal to 0.5. The effect of confinement due to friction between the loading plates and the specimen is also obvious.

Figure 17 shows the stress contours (σ_x, σ_y, τ_{xy}) in case where ν is equal to 0.5. For σy, it is obvious that the effect of confining stresses leads to increasing the vertical stress near the center of the specimen and reducing the vertical stress near the prism edges of the specimen. However, the effect of Poisson's ratio on vertical stresses is not large. In case of σx, it is obvious that the effect of confining stress is maximum near the loading plates, because of friction, and this effect vanishes in the middle of the specimen. Shear stresses, τ_{xy}, is maximum near the loading plates, because of friction, and this effect disappears at the center line of the beam and away from the loading plates. However, the stress values are slightly affected near the edges because of edge effects. This effect does not appear in the FEM as the Poisson's ratio effect is included in the stress-strain relation not by indirect way as in the proposed method.

The last verification example is for a RC column subjected to uniform compression loading. Analysis is performed assuming elastic material properties. The objective of this study is to show that the confinement effects caused by existence of stirrups are automatically taken into account. The column dimensions, reinforcement properties and element arrangement used in the analysis are shown in

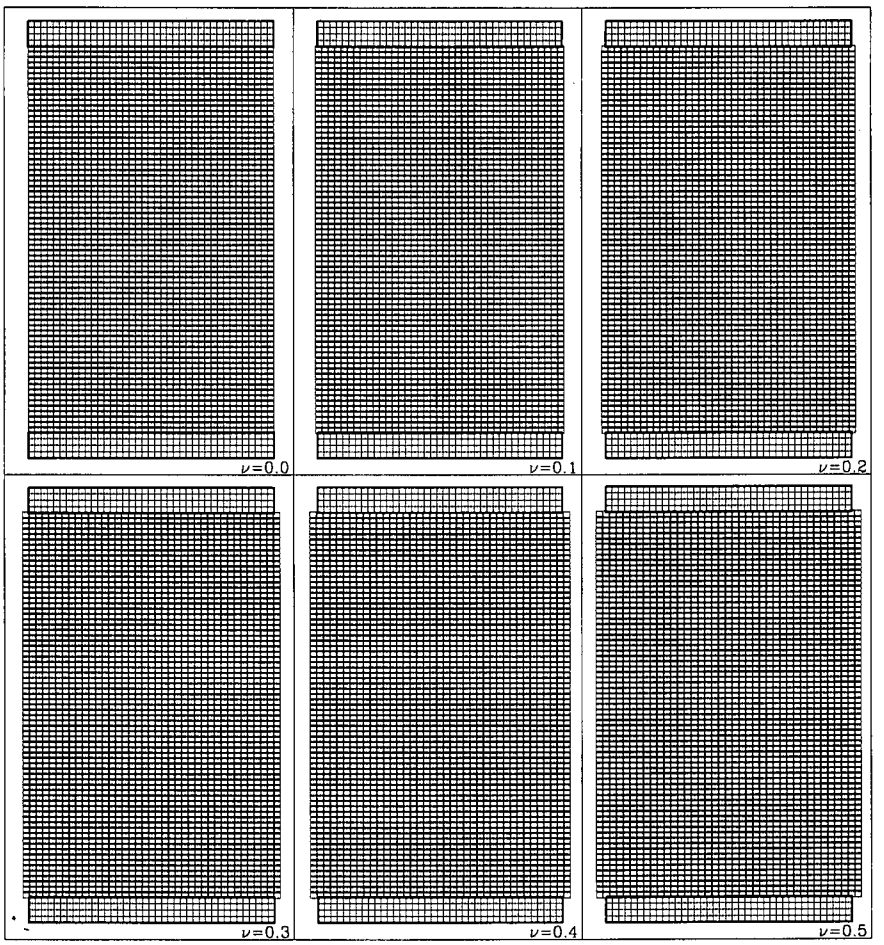

Fig. 14 Deformed shape of specimens with different Poisson's ratios and subjected to uniform compression (without friction, Illustration scale Factor=50)

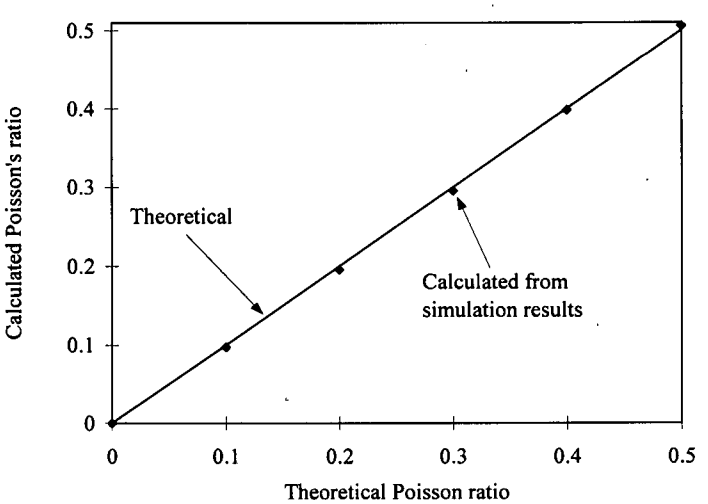

Fig. 15 Comparison between theoretical and calculated Poisson's ratio

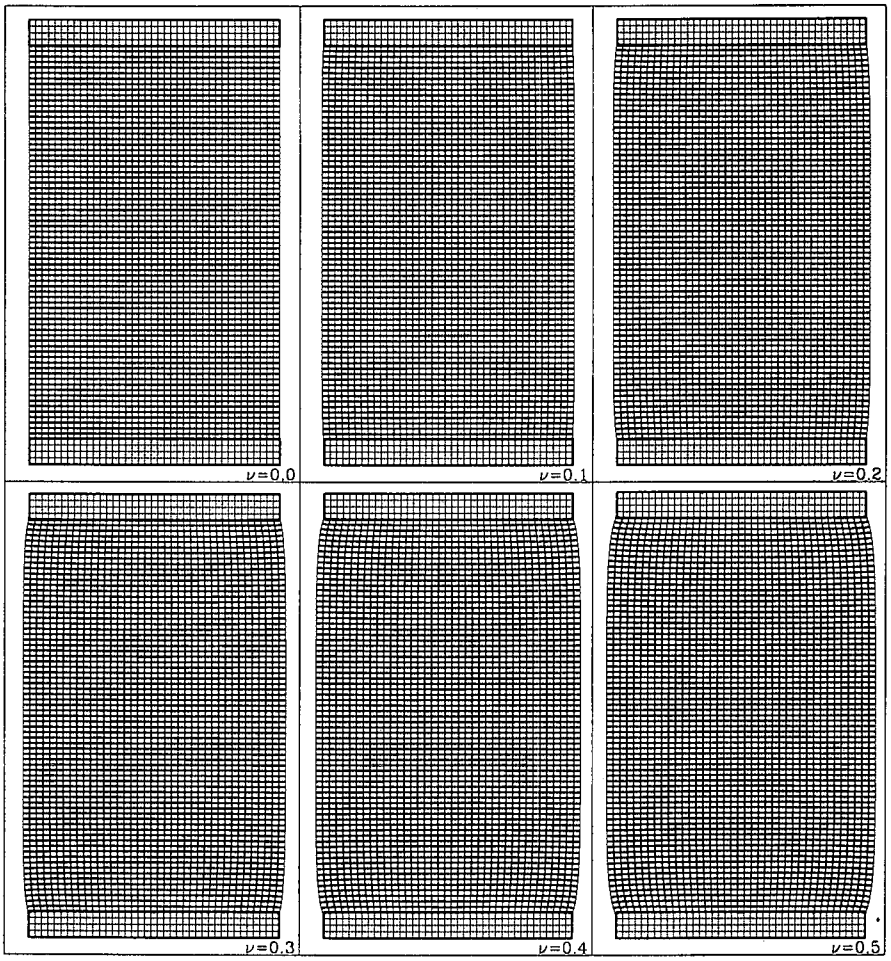

Fig. 16 Deformed shape of specimens with different Poisson's ratios under uniform compression (with friction, Illustration scale Factor=50)

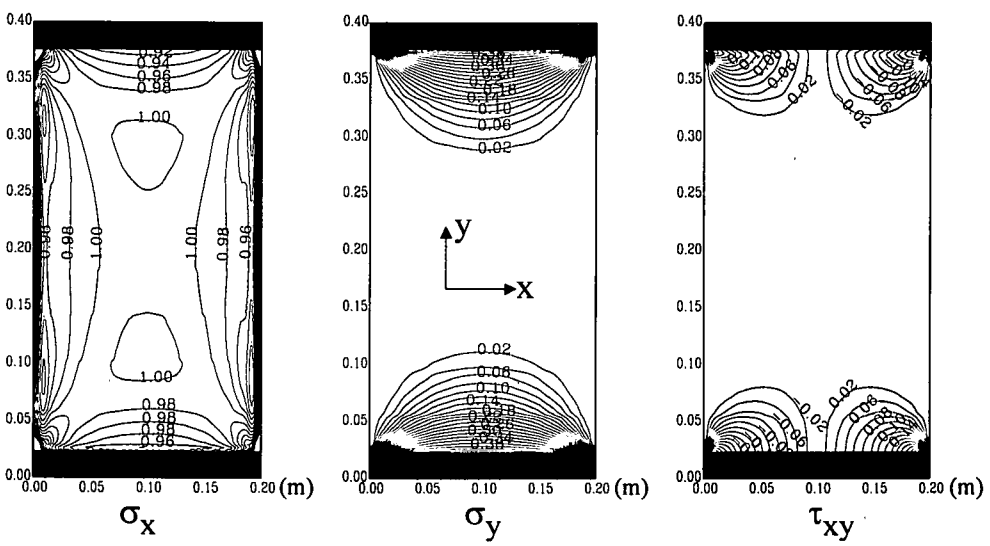

Fig. 17 Stress contour of specimen under uniform compression (Poisson's ratio, v=0.5, with friction) (stresses are normalized by the applied axial stress at the edge of the specimen)

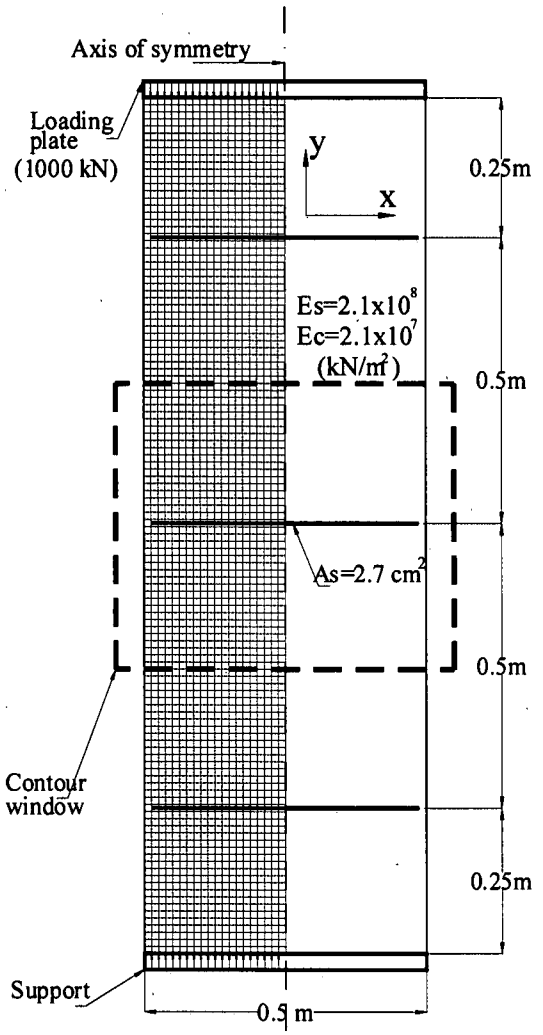

Fig. 18 Dimensions, reinforcement and element arrangement

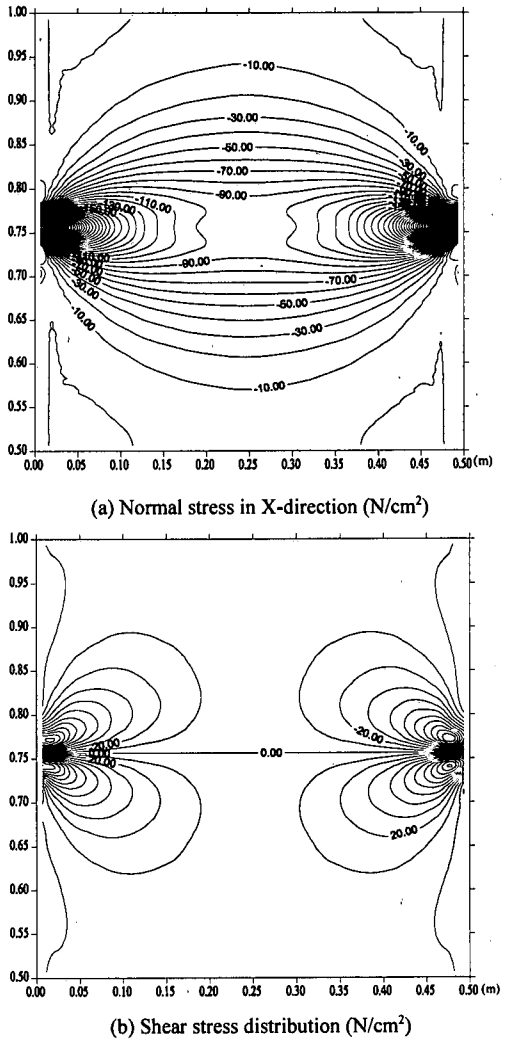

Fig. 19 Stress contour arround the reinforcement bar location

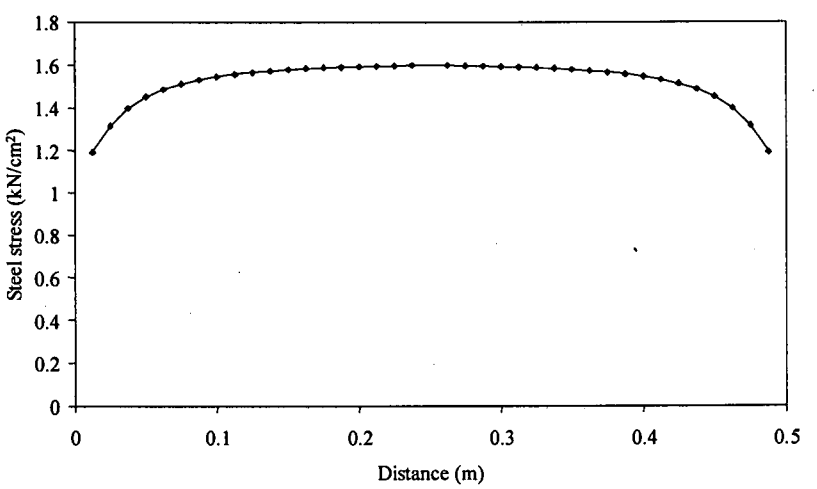

Fig. 20 Normal stress distribution at the reinforcement bar

Fig.18. Simulation is performed for only half of the column because of symmetry and using 2,400 square shaped elements. The Poisson's ratio is assumed 0.3. The analysis is performed under the assumption of 2-dimensional behavior and plane stress condition.

The simulation results are shown in **Figs. 19** and **20**. **Figure 19** shows the variation of stresses due to existence of reinforcement bar. It is obvious that the concrete is subjected to compressive lateral stresses due to the reinforcement bar. These stresses increase in the vicinity of the bar and decrease away from the bar location. As the lateral bar prevents the lateral displacement of the column, compression and shear stresses are maximum at the reinforcement bar end. **Figure 20** shows the variation of reinforcement bar stress within the column width. It is noticed that the bar stresses are mainly tension. The tensile stresses decreases till reaching the bar end. Reinforcement bar stresses should be zero at the end of the bar from theoretical point of view. As the stress gradient at the bar ends is very steep, tensile stresses at the bar ends could not be calculated accurately. To overcome this problem, elements of smaller size should be used.

7. CONCLUSIONS

A simple and efficient technique termed Applied Element Method, AEM, for structural analysis is introduced and applied to several fundamental structures made by linear material to verify accuracy of the model. Background and outline of the AEM are also explained. From the numerical results obtained, it was proved that the AEM has the following advantages, in elastic analysis:

1. Displacement can be calculated accurately if the element size is small.
2. Internal stresses can also be obtained accurately.
3. Elements with small size should be used in shear dominant cases to get accurate shear stresses.
4. In case of high stress gradients, like in case of concentrated loads, elements of small size should be used to follow the stress changes.
5. Elements of large size can be used in case of slender frames without significant changes in the calculated normal stresses.
6. The number of connecting springs should be large if the element size is relatively large.
7. The Poisson's ratio effect can be considered accurately without significant increase in the time of the analysis. Simulation results are compared with the theoretical ones and the results are of good accuracy.
8. The formulations introduced in the paper are for rectangular elements with and without reinforcements set parallel to element edges, and for Poisson's ratio using square elements. However, this is not the limitation of the method. The AEM can utilize elements of general shape, after modifications of the formulas used.

Having good results in elastic analysis encourages us to extend the applicability of the proposed model to the nonlinear case. Some of the results are introduced in following publications (Refs.10-14).

REFERENCES

1) Architectural Institute of Japan: A report on damage during Miyagiken-Oki Earthquake of 1978, 1979 (in Japanese).
2) Nishimura, A., Ueno, Y., Fujiwara, S., Ijiri, I., Fukunaga, T., Hishida, S., Hatake, K., Tanegashima, A., Kinoshita, H., Mizoi, Y. and Tatsuno Y.: Typical traumatic cases of the Great Hanshin Earthquake, Advances in Legal Medicine 3, pp.350-353, July 1997.
3) Okamura, H. and Maekawa, K.: Nonlinear analysis and constitutive models of reinforced concrete, Gihodo Co. Ltd., Tokyo, 1991.
4) Kawai, T.: Recent developments of the Rigid Body and Spring Model (RBSM) in structural analysis, Seiken Seminar Text Book, Institute of Industrial Science, The University of Tokyo, pp. 226-237, 1986.
5) Meguro, K. and Hakuno, M.: Fracture analyses of structures by the modified distinct element method, Structural Eng./Earthquake Eng., Vol. 6. No. 2, 283s-294s., Japan Society of Civil Engineers, 1989.
6) Meguro, K. and Hakuno, M.: Application of the extended distinct element method for collapse simulation of a double-deck bridge, Structural Eng./Earthquake Eng., Vol. 10. No. 4, 175s-185s., Japan Society of Civil Engineers, 1994.
7) Kikuchi, A., Kawai, T. and Suzuki, N.: The rigid bodies-spring models and their applications to three dimensional crack problems, Computers & Structures, Vol. 44, No. 1/2, pp. 469-480, 1992.
8) Ueda, M. and Kambayashi, A.: Size effect analysis using RBSM with Vomori elements, JCI (Japan Concrete Institute) International Workshop on Size Effect in Concrete Structures, pp. 199-210, 1993.
9) Tagel-Din, H.: A new efficient method for nonlinear, large deformation and collapse analysis of structures, Ph.D. thesis, Civil Eng. Dept., The University of Tokyo, Sept. 1998.
10) Meguro, K. and Tagel-Din, H.: A new simplified and efficient technique for fracture behavior analysis of concrete structures, 3rd International Conference on Fracture Mechanics of Concrete and Concrete Structures (FRAMCOS-3), Gifu, Japan, 1998.
11) Meguro, K. and Tagel-Din, H.: Simulation of buckling and post-buckling behavior of structures using Applied Element Method, Bulletin of Earthquake Resistant Structure, IIS, University of Tokyo, No. 32, pp. 125-135, 1999.
12) Meguro, K. and Tagel-Din, H.: Development of a new fracture analysis method with high accuracy based on discontinuous material modeling, 16th annual Conf. on Natural Disaster Reduction, Osaka, Japan, 1997.
13) Tagel-Din, H. and Meguro, K.: Applied element simulation for collapse analysis of structures, Bulletin of Earthquake

Resistant Structure, IIS, University of Tokyo, No. 32, pp.113-123, 1998.
14) Tagel-Din, H. and Meguro, K.: Analysis of a small scale RC building subjected to shaking table tests using Applied Element Method, Proceedings of the 12th World Conference on Earthquake Engineering, January 30th-February 4th, 2000.

(Received March 15, 1999)

応用要素法：基本理論と線形材料への適用

目黒公郎・タグエルディン-ハテム

著者らは，構造物の大変形問題や完全に崩壊に至るまでの挙動を，高い精度でしかも適正な計算時間で解析することを目的に，新しい構造解析手法(応用要素法)の開発を進めている．提案モデルでは，解析対象媒質や構造物は仮想的に分割された小要素の集合体として考え，各要素の辺同士は法線方向と接線方向にそれぞれ分布型のばねで結合されている．本研究では，モデル構築の第一歩として行った線形材料の微小変形領域を対象とした基本理論の構築と定式化について紹介し，さらに提案モデルを用いた解析結果と理論解を比較することでその高い精度を確認した．